AFOSR-TR- 88 1019

Electromagnetic Cross Sections of Conductive Fibers:

Modified Drude Equations

and

Dependence of Dielectric Constant on Particle Size

Final Report

Contract No. F49620-87-C-0051

Prepared by

N. E. Pedersen
P. C. Waterman
J. C. Pedersen

August 31, 1988

PANAMETRICS, INC.
221 Crescent Street
Waltham, Massachusetts 02254

Submitted to

Dr. Liselotte Schioler
Air Force Office of Scientific Research
Directorate of Electronic and Material Science
Spacecraft Survivability Program
Building 410
Bolling Air Force Base, DC 20332-6448

DTIC
ELECTE
S OCT 0 6 1988
D
H

88 10 5 290

199873

REPORT DOCUMENTATION PAGE

1a. REPORT SECURITY CLASSIFICATION	1b. RESTRICTIVE MARKINGS
2a. SECURITY CLASSIFICATION AUTHORITY	3. DISTRIBUTION/AVAILABILITY OF REPORT
2b. DECLASSIFICATION/DOWNGRADING SCHEDULE	Approved for public release; distribution unlimited.
4. PERFORMING ORGANIZATION REPORT NUMBER(S)	5. MONITORING ORGANIZATION REPORT NUMBER(S)
	AFOSR-TR- 88-1019

6a. NAME OF PERFORMING ORGANIZATION	6b. OFFICE SYMBOL (If applicable)	7a. NAME OF MONITORING ORGANIZATION
Panametrics Inc		AFOSR/NE

6c. ADDRESS (City, State and ZIP Code)	7b. ADDRESS (City, State and ZIP Code)
221 Crescent Street Waltham, MA 02254	Bldg 410 Bolling AFB DC 20332-6448

8a. NAME OF FUNDING/SPONSORING ORGANIZATION	8b. OFFICE SYMBOL (If applicable)	9. PROCUREMENT INSTRUMENT IDENTIFICATION NUMBER
AFOSR	NE	F49620-87-C-0051

8c. ADDRESS (City, State and ZIP Code)	10. SOURCE OF FUNDING NOS.			
Bldg 410 Bolling AFB DC 20332-6448	PROGRAM ELEMENT NO.	PROJECT NO.	TASK NO.	WORK UNIT NO.
	61102F	2306	A3	

11. TITLE (Include Security Classification) Electromagnetic Cross Sections of Conductive Fibers: Modified Drude Equations and Dependence of Dielectric Constant on Particle Size

12. PERSONAL AUTHOR(S) Pedersen, Waterman, Pedersen

13a. TYPE OF REPORT	13b. TIME COVERED	14. DATE OF REPORT (Yr., Mo., Day)	15. PAGE COUNT
Final	FROM 5 Apr 87 TO 15 Jun 88	AUG 31 88	

16. SUPPLEMENTARY NOTATION

17. COSATI CODES			18. SUBJECT TERMS (Continue on reverse if necessary and identify by block number)
FIELD	GROUP	SUB. GR.	

19. ABSTRACT (Continue on reverse if necessary and identify by block number)

Our ability to compute the electromagnetic scattering, absorption, and extinction cross sections of randomly oriented electrically conducting thin fibrous particles has improved substantially over the past five years or so. This has been made possible by a number of Government contracts, including AFOSR, and a continuing in-house effort at Panametrics. Although some obvious limitations are imposed by the use of a too-simple current function, the effects of these are known, easily recognized, and can be dealt with.

20. DISTRIBUTION/AVAILABILITY OF ABSTRACT	21. ABSTRACT SECURITY CLASSIFICATION
UNCLASSIFIED/UNLIMITED ☐ SAME AS RPT. ☐ DTIC USERS ☐	UNCLASSIFIED

22a. NAME OF RESPONSIBLE INDIVIDUAL	22b. TELEPHONE NUMBER (Include Area Code)	22c. OFFICE SYMBOL
SCHIOLER	(202) 767-4933	NE

DD FORM 1473, 83 APR   EDITION OF 1 JAN 73 IS OBSOLETE.

SECURITY CLASSIFICATION OF THIS PAGE

TABLE OF CONTENTS

Accession For

NTIS GRA&I	☑
DTIC TAB	☐
Unannounced	☐
Justification	

By

Distribution/

Availability Codes

| Dist | Avail and/or Special |
| A-1 | |

i

LIST OF ILLUSTRATIONS

LIST OF TABLES

1.0 INTRODUCTION

Our ability to compute the electromagnetic scattering, absorption, and extinction cross sections of randomly oriented electrically conducting thin fibrous particles has improved substantially over the past five years or so. This has been made possible by a number of Government contracts, including AFOSR,[1] and a continuing in-house effort at Panametrics. Although some obvious limitations are imposed by the use of a too-simple current function, the effects of these are known, easily recognized, and can be dealt with.

A rather more severe limitation has been our inability to adequately characterize the complex dielectric constant of these particles in the infrared wavelength range below ~50 or so microns. The problems are twofold:

(a) We have been using the Drude (as improved by Sommerfeld)[2] theory for predicting dielectric constant. Although this works well in the case of most metals, serious errors arise for wavelengths sufficiently short for the onset of quantum effects. Although the experimental data for dielectric constant in general retain the characteristics of the simple Drude model, large quantitative differences are more than common at the shorter infrared wavelengths.

(b) When the fiber diameter is on the order of, or smaller than the electron mean free path in the bulk material, inelastic collisions with the surface of the (very thin) particle reduce the effective value of the mean free time τ and the mean free path. This in turn gives rise to serious errors in the Drude predictions even in the wavelength range where they would otherwise be accurate.

1

Either of the above problems by itself would not be very difficult to address. In (a) alone, we would simply incorporate the experimentally derived data tables into our computer programs and do appropriate interpolation. The case (b) alone, we would employ existing and long standing theoretical results that predict the size dependent change in electrical conductivity of very thin wires. The results of this treatment, as well as the elements of the Drude/Sommerfeld treatment, will be discussed in the following Section.

The problem arises when the diameter is sufficiently small that we need to apply both kinds of correction to the same particle. If we use the above purely empirical method for obtaining the complex dielectric constant, we lose our ability to intelligently utilize the results of the small diameter conductivity correction. This correction involves the modification of dielectric constant due to a change in mean free time r from the bulk value. The purely empirical approach renders such a correction impossible.

We have chosen to deal with this somewhat perplexing problem by selecting a middle ground:

We have found it is possible to individually modify the two Drude equations for very good fits to the experimentally derived data. This retains the meaning of relaxation time, although we realize that it is over simplified. The size corrections, if required, can then be applied to these Modified Drude equations.

The above approach is not a particularly happy one, but (short of an overwhelming quantum treatment), we believe that it represents the most reasonable compromise. Note that this problem arises only when the small diameter correction (less than -100 Angstroms) is needed. The details of the analysis will be discussed in Section 3.0.

2.0 ELECTRONIC PROPERTIES OF METALS

2.1 Simple Model for the Dielectric Constant of Metals

In order to be able to apply our computations to the infrared and visible, as well as the microwave case, it is necessary to build in the optical behavior of the fibers. In addition, in order to include extremely small fiber diameters, the dependence of the electrical conductivity upon particle radius must be included. These effects will now be considered.

In recent work by Ordal et al.,[3] the Drude model for the prediction of the complex optical dielectric constant was compared with experimentally measured values for fourteen metals (Al, Co, Cu, Au, Fe, Pb, Mo, Ni, Pd, Pt, Ag, V, W). The model, which is based on the free electron theory of metals, is found to be in surprisingly good agreement with measurements at the longer infrared wavelengths, even for the case of some of the transition elements such as Fe.

In brief outline, the free electron theory runs as follows. The equation of motion for the single electron is[4]

$$m^* \ \frac{dv}{dt} + \frac{1}{\tau_b} v \ = eE \qquad\qquad (2.1)$$

with m^*, e the electron effective mass and charge, E the applied electric field, and τ_b the bulk material relaxation time (average time between collisions). For a sinusoidal applied field $E \, e^{i\omega t}$, one then obtains a velocity $v e^{i\omega t}$, where

$$v = \frac{(e/m^*) \ \tau_b \ E}{1 + i\omega\tau_b} \ .$$

The corresponding current density j is given by

$$j = nev = \frac{(ne^2 \ \tau_b/m^*) \ E}{1 + i\omega\tau_b}$$

3

where n is the electron density. But one also has

$$j = \sigma_b E$$

in terms of the bulk static conductivity σ_b, and comparing these last equations gives (setting $\omega = 0$)

$$\sigma_b = n\ e^2\ \tau_b/m^* \quad . \tag{2.2}$$

In the context of the Drude model the complex dielectric constant, required as an input to the fiber scattering computation, has the form

$$\epsilon = \epsilon' + i\epsilon'' \quad , \tag{2.3}$$

where

$$\epsilon' = \epsilon_\infty - \frac{\sigma\tau}{\epsilon_0}\ \frac{1}{1 + (\omega\tau)^2} \quad , \tag{2.4a}$$

$$\epsilon'' = \frac{\sigma}{\omega\epsilon_0\ [1 + (\omega\tau)^2]} \quad . \tag{2.4b}$$

Here ϵ_∞ is the high-frequency limiting value of the dielectric constant (we will generally assume $\epsilon_\infty = 1$). Note carefully that we have now allowed for the possibility that the conductivity and relaxation time may be reduced by fiber size effects to be discussed below, by writing σ, τ. The reductions are proportional, so that $\sigma/\sigma_b = \tau/\tau_b$, and one has as before

$$\sigma = n\ e^2\ \tau/m^* \quad . \tag{2.5}$$

As already noted, the Drude model has been fit by Ordal and co-workers for a number of metals,[3] by comparison with experimental infrared measurements of their own, as well as those of other workers, using Kramers-Kronig analysis along with other

4

techniques. We employ r_b values that follow from their Table I. It is interesting to note from the table that their corresponding values of resistivity for the most part do not differ greatly from the Handbook values.

It may be necessary to reduce the value of r from that corresponding to bulk material. When one or more dimensions of a conductive material (metal or semiconductor) are of the order of the mean free path Λ of the conduction electrons, collisions with the surface will significantly reduce Λ. Assuming Fermi-Dirac statistics, this will result in a corresponding reduction of the relaxation time due to the relation

$$\Lambda = v_F r , \tag{2.6}$$

where v_F is the Fermi velocity. Note that, in consequence of Eq. (2.5), the conductivity is also reduced.

The classic early work on this subject was done in 1938 by Fuchs, who considered thin films.[5] In a more recent paper, Dingle extended the analysis to circular wires,[6] providing useful analytical and numerical results which we employ as follows. First, define the quantity $k = 2a/\Lambda$ as the ratio of fiber diameter to mean free path. We also write ϵ for the probability of elastic collision occurring at the surface (this should not be confused with the dielectric constant; from the context it will be clear which quantity is involved). Note that only inelastic collisions are effective in determining the reduced mean free path; consequently, no size effects will be present when $\epsilon = 1$.

The detailed analytical results given by Dingle would require lengthy computer analysis. Rather than programming these formulas, we find it more convenient to employ a combination of tabulated results along with asymptotic formulas in the following manner.

In the simplest case $k \gg 1$ and the size effect gives only a perturbation on the bulk values. For the reduction factor, which Dingle writes in terms of the conductivity ratio σ/σ_b, we then take

$$\frac{\sigma}{\sigma_b} = 1 - \frac{3\,(1-\epsilon)}{4\,k} \quad , \quad k > 10 \tag{2.7}$$

Note that this ratio goes to unity when $k \longrightarrow \infty$, as required.

In the other extreme, when $k \ll 1$, the effect is large. Using Dingle's limiting formula for this case we take

$$\frac{\sigma}{\sigma_0} = \left(\frac{1+\epsilon}{1-\epsilon}\right) k - \frac{3k^2}{8}\left[\frac{(1 + 4\epsilon + \epsilon^2)}{(1-\epsilon)^2}\,(\ln 1/k + 1.059)\right.$$

$$\left. - (1-\epsilon)^2 \sum_{1}^{\infty} n^3\,\epsilon^{n-1}\ln n\right]\frac{-2k^3}{15}\,\frac{(1 + 11\epsilon + 11\epsilon^2 + \epsilon^3)}{(1-\epsilon)^3} \quad ,$$

$$k < 1/10. \tag{2.8}$$

Finally, for the intermediate cases $1/10 \leq k \leq 10$, we employ the values listed in Table 4 of Dingle, along with linear interpolation. In all cases computations are only carried out for $\epsilon = 0, 1/2, 1$ (of course, when $\epsilon - 1$ all electron-wall collisions are elastic and no reduction occurs). In view of the uncertainty of ϵ in the first place, this seems a reasonable selection to demonstrate the possibilities.

6

2.2 Electronic Properties of Carbon Fibers

Carbon fibers can be prepared with high length-to-diameter ratios, they are robust, and have electrical properties which are suitable for this application. Higher electrical conductivities can be obtained by intercalation or metal coatings. The status of these materials for obscuration applications was considered by Dresselhaus, Goldberg and Spain.[7] This section will consider only pristine fibers, and review in greater depth the parameters of interest for electromagnetic interaction (electrical conductivity, σ, density of carriers, n, relaxation time, τ, and mean-free path for scattering, Λ, just as in the metallic case.

It is emphasized that carbon differs from typical metals since the Fermi energy is small (typically $\lesssim$ 0.1 eV), and also the effective mass $\sim$0.01 m_O, so that the density of carriers is orders of magnitude smaller than that of metals (for which n $\sim 10^{25}$ m^{-3}), and can vary appreciably with temperature and the concentration of defects and impurities in the material. Since carbon fibers are defective materials, it is found that their properties vary enormously with preparation conditions. Accordingly, this report will commence with a brief discussion of fiber types and preparation parameters.

There are two types of high-strength carbon fibers. The first kind is prepared by the heat-treatment of a polymer blend, and comprises the bulk of the commercial market. Of these, ex-PAN (poly-acrylo-nitrile) fibers account for over 90% of the market. Ex-pitch fibers are used in applications where high elastic modulus is needed, and current research is aimed at preparing lower modulus types with properties similar to those of high-strength ex-PAN. The diameters of ex-polymer fibers are usually 7-10 μm, and lengths are continuous, so that chopped fibers can be prepared with well-defined aspect ratios.

The second type is prepared by the catalytic chemical vapor deposition of hydrocarbons, called CCVD filaments hereafter. The

diameters of these filaments are controlled by the diameter of the catalyst particle (see Figure 2.1), and by deposition conditions. In particular, the temperature-time-partial pressure conditions can determine whether the filaments are thickened or not. Fairly straight filaments can be produced by this method, with diameters ranging from about 10 nm to 100 μm. High aspect ratios (e.g., > 1000) are possible. Both types of fibers are discussed in detail in Dresselhaus, Dresselhaus, Sugihara, Spain and Goldberg.[8]

Figures 2.2, 2.3 and 2.4 illustrate typical data of the resistivity as a function of temperature (4-300°K) for ex-PAN fibers compared to anthracene chars (Fig. 2.2), ex-mesophase pitch compared to single crystal graphite (Fig. 2.3), and CCVD filaments compared to single crystal graphite (Fig. 2.4). The curves are labelled by the temperature of heat-treatment (T_{HT}). This is an important preparation parameter which is used to improve the structural characteristics. Ex-polymer fibers and CCVD filaments are produced by processes which are typically in the temperature region below about 1200°C. Subsequent heat-treatment at T_{HT} for a period of time such as 10 minutes changes their structural characteristics and physical properties, as typified by the electrical resistivity curves in Figs. 2.2-2.4.

The most important structural change that occurs during this heat-treatment concerns the manner in which the hexagonal carbon layers are stacked with respect to each other. In perfect graphite the layers are stacked in a regular ABAB .... sequence. Ex-polymer fibers heat-treated to less than 1200°C have nearly a random interlayer correlation, and are called turbostatic carbon. Further heat-treatment increases the correlation. It is found that fibers have a tendency to graphitize (graphitization is the process by which the interlayer correlation is developed) in the order CCVD filaments, ex-pitch fibers, ex-PAN fibers. This tendency is seen in the Figs. 2.2-2.4, where resistivities are progressively lower for a given value of T_{HT} in the order of greater graphitization.
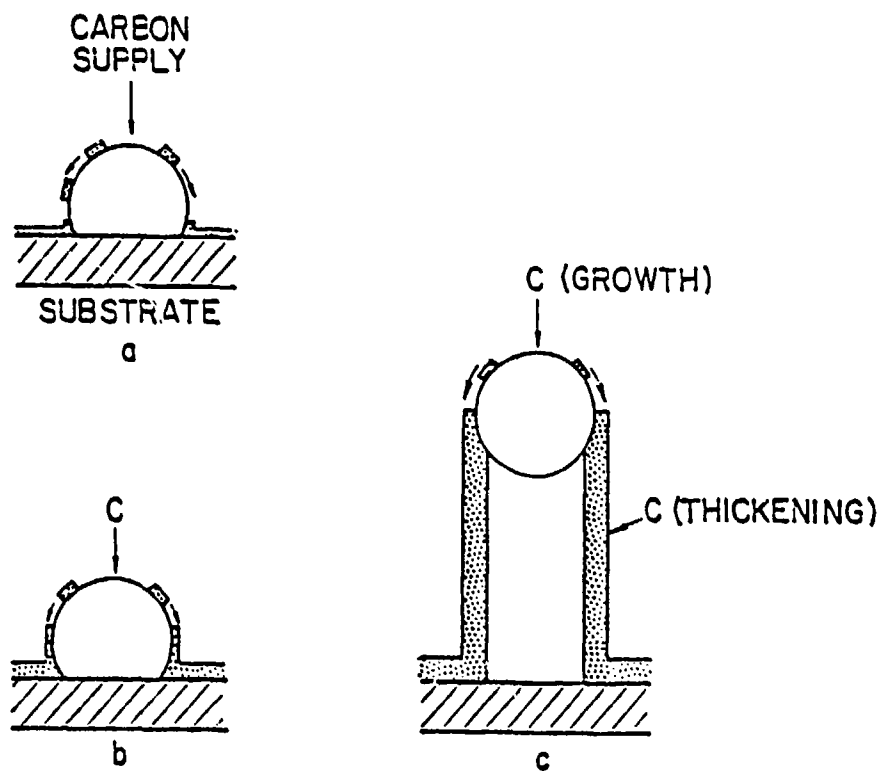
Figure 2.1 A schematic of the growth of a CCVD filament from
catalytic deposition of carbon on a catalyst
particle. The diameter of the initial filament
is controlled by the size of the catalyst particle,
but carbon can be deposited on the sides of the
filaments later, thereby thickening them.

9
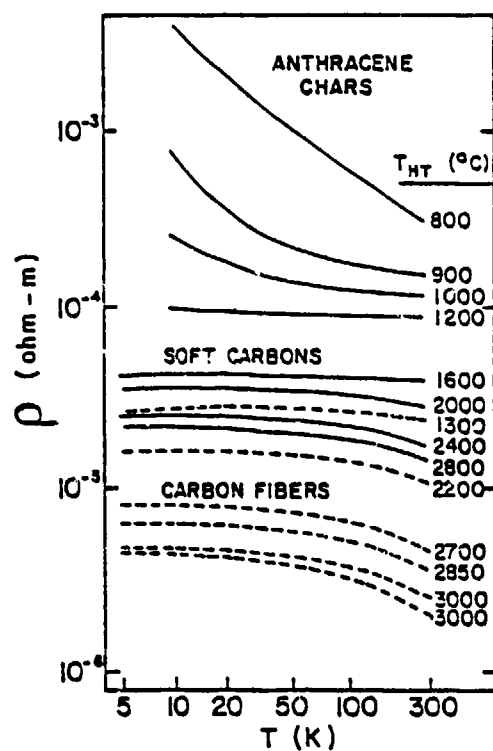
Figure 2.2 A comparison of the temperature dependence
of the electrical resistivity of ex-PAN
fibers compared to chars of anthracene
(from Spain et al., ref. 9).
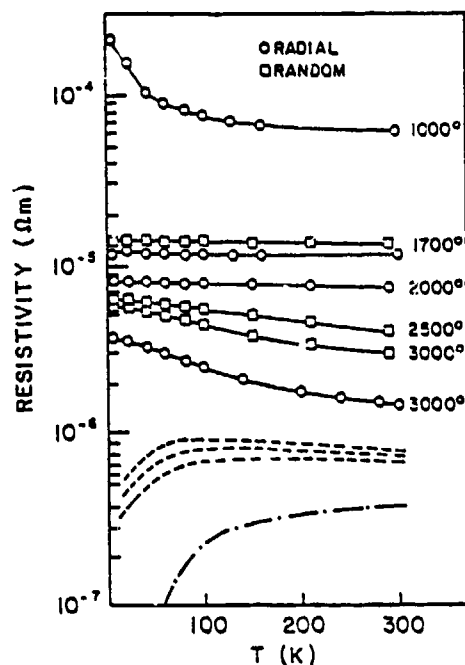
Figure 2.3   The temperature dependence of the resistivity
              of ex-pitch fibers compared to single crystal
              graphite.   Also included are data for whiskers,
              which are highly graphitic filaments found in
              certain carbon arc-processes.   (Data from
              Bright, ref. 12).

11
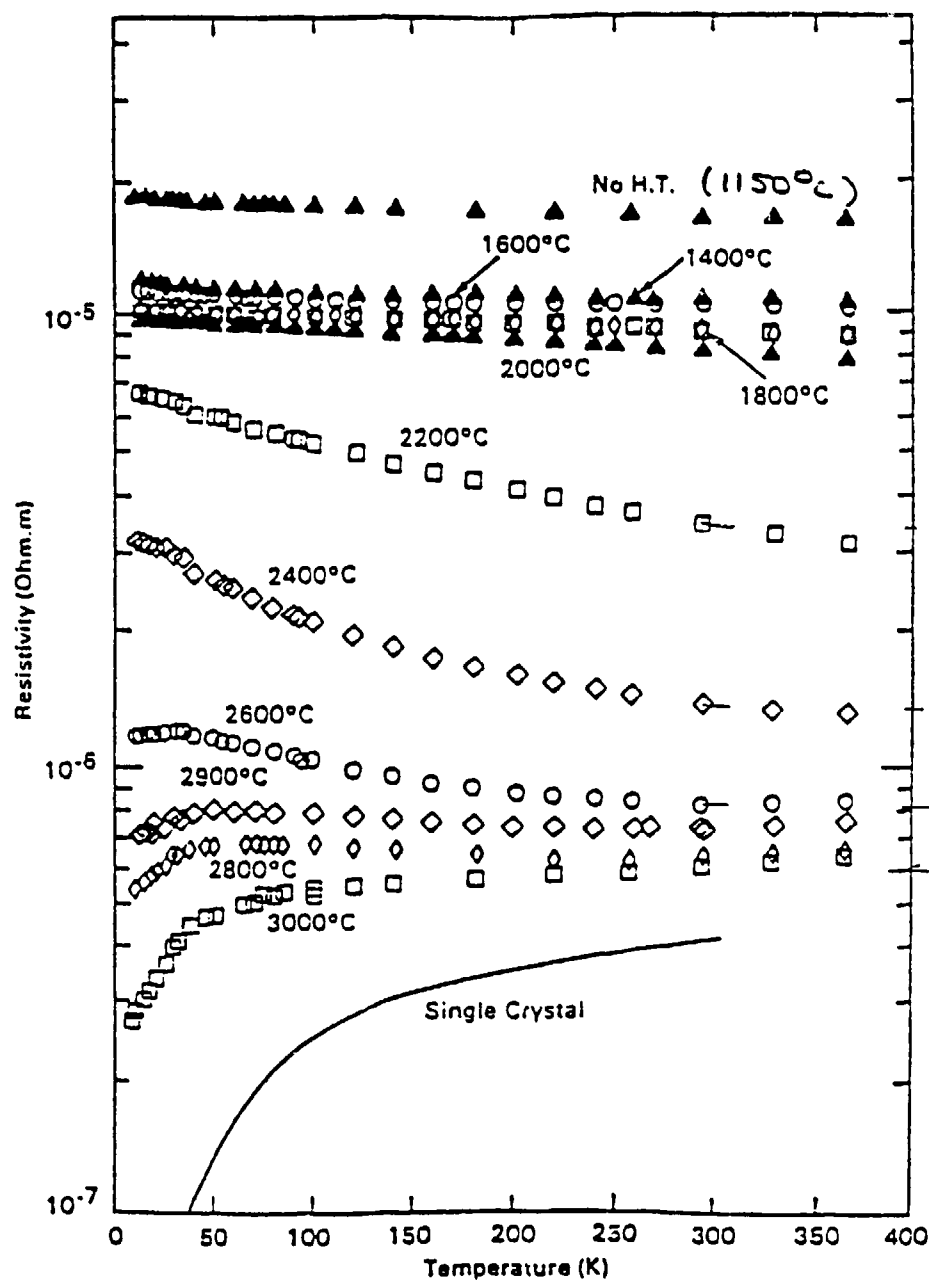
Figure 2.4 The temperature dependence of the resistivity
of CCVD filaments compared to single crystal
graphite. (Data from Heremans, ref. 10).

Other structural defects are present in these materials (see Dresselhaus et al. for discussion)[7], but it is remarkable that the electrical properties appear to be similar for fibers or bulk carbons with the same resistivity. Thus, the parameters of interest for electromagnetic interactions can be discussed without recourse to details of fiber type.

The electrical resistivity characteristics between about 4-300°K have already been presented in Figs. 2.2-2.4. A few results have also been obtained at high temperature. Figure 2.5 presents data on two types of CCVD filaments to 2000°C, from which it may be seen that carbon has a lower specific resistivity than any of the refractory metals above about 1000°C. The higher temperature data in Fig. 2.6 were obtained using a 28 us pulse, with temperatures estimated from thermophysical data. This allowed studies to be carried out on CCVD filaments with T_{HT} as low as 1700°C without appreciable changes in properties due to structural rearrangement.

An mentioned above, the fibers represented in Figs. 2.2-2.6 cover a range from nearly turbostatic, to nearly graphitic carbon. It is difficult to analyze the resistivities without making assumptions and simplifications, but a reasonably consistent picture has been developed. It is most convenient to divide into three regions:

a) Graphitic - In this case the band model is well developed with a complicated energy-wavevector relationship (see Dresselhaus et al. for a review and extensive references)[7]. The densities of electrons and holes are usually taken to be equal (the Fermi energy takes its intrinsic value). The magnetoresistance can be used to estimate the mean carrier mobility using the "simple two band model" (STBM). This mobility is controlled by phonon scattering in single crystals, but boundary scattering needs to be included using Matthiesson's rule for fibers. The speed of carriers

13
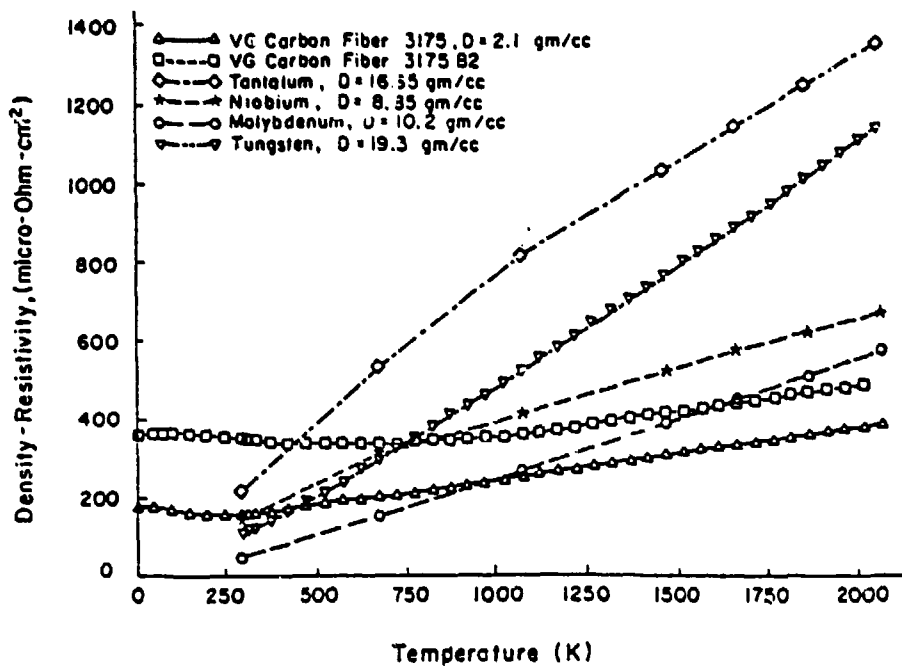
Figure 2.5   The high temperature DC resistivity of CCVD
filaments compared to refractory metals. (Data
from Woollam, 1987, to be published).
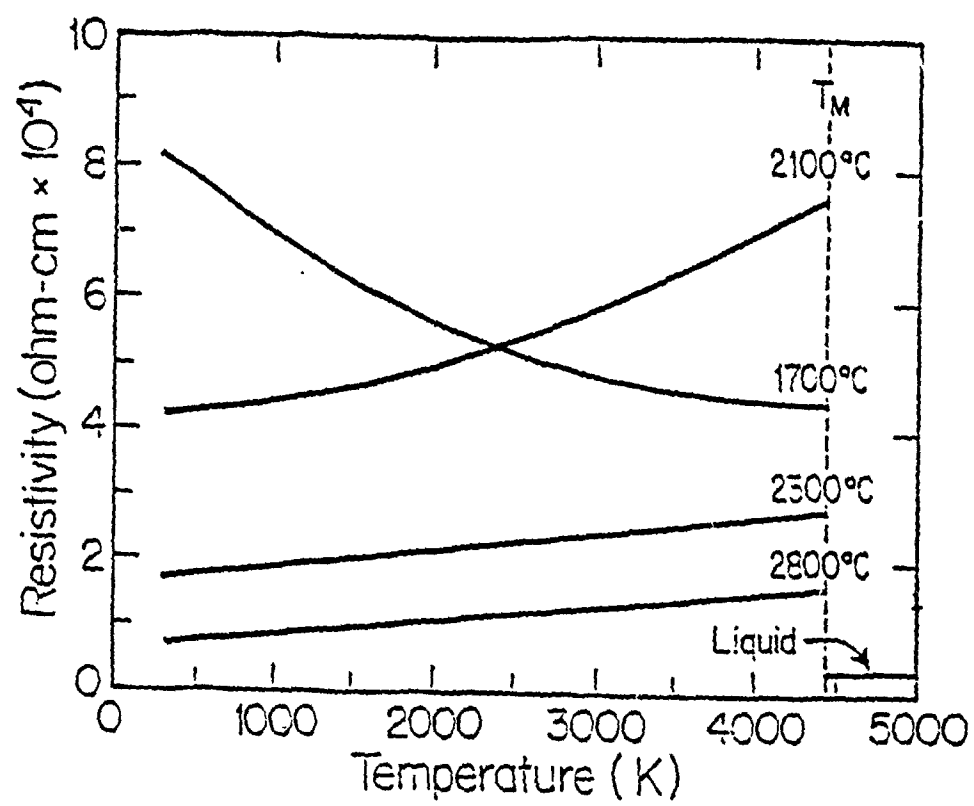
Figure 2.6 High temperature resistivity of CCVD filaments from a pulse method. (Data from Heremans et al., ref. 11).

with the Fermi energy, v_F, along the graphite planes varies strongly with wavevector. Values range from $0 - 10^6$ m/s, and a mean value is about 5×10^5 m/s. Only some CCVD filaments (such as those prepared from benzene) are in this category.

b)   Turbostatic Fibers - In this case a very simple dispersion relationship can be used which is appropriate to a single layer plane of carbon atoms. The carrier speed is independent of wavevector, and equal to approximately 10^6 m/s. However, the magnetoresistance cannot be used to estimate the mobility, and the resistivity-temperature curves are usually analyzed assuming a temperature-independent mobility. Values of the mean-free path are compared with values of the "mean crystallite dimension", L_a.

c)   Intermediate Case - This is the actual case for most ex-polymer and CCVD filaments, and is treated using the Simple Two-Band Model allowing the density of electrons and holes to differ (i.e., allowing the Fermi energy to take values different from intrinsic). The model can be used to analyze the data in several ways. The predominant carriers are usually holes, since acceptors depress the Fermi energy. The mean-free path is again compared to L_a values from structural analysis.

The simple two-band model will be described briefly, and analysis of experimental data using it will follow.

The Simple Two-Band Model (STBM)

The simple two-band model simplifies the complex dispersion relationship obtained for single-crystal graphite, and replaces it with a conduction and valence band in which the carriers re restrained to motion along the layer planes. The dispersion of the effective mass in the basal directions is also replaced by an average mass for each band. In practical situations the electrons and holes are given equal masses, and the parameters that are variable are the overlap of the bands, Δ, the effective mass, m^*, and the Fermi energy, E_F. The total density of electrons, n, and holes, p, are then:

$$n = Ck_BT\ln(1 + \exp(E_F/k_BT))\qquad(2.9)$$

and p is the same expression with E_F replaced by $(\Delta - E_F)$, and

$$C = 2m^*/n\tilde{c}h^2.\qquad(2.10)$$

where $\tilde{c}$ is the interlayer spacing (approximately 0.335-0.345 nm). As explained above, Spain et al.[9] used this model to analyze data for ex-PAN fibers, fixing the effective mass $(0.012m_0)$, and allowing E_F and Δ to be determined by least squares fits to the resistivity-temperature plots. In their calculations the carrier mobility was assumed independent of temperature. Heremans analyzed data on CCVD filaments with higher mobilities for which the approximation of a constant mobility was not appropriate.[10] He therefore assumed that the densities of electrons and holes were equal (equivalent to $E_F = \Delta/2$), assumed a value of C equivalent to taking $m^* = 0.013m_0$, and fixed $E_F = 9$ meV.

The mobility, relaxation time and mean-free path for scattering are calculated using the simple formulae

$$\mu = 1/(n+p)e\,\rho \qquad (2.11)$$

$$\tau = \mu m^*/e. \qquad (2.12)$$

$$\Lambda = v_F \tau. \qquad (2.13)$$

Although this model represents a simple approximation to a complex situation, the trends in electronic parameters are reasonable, and values give reasonable agreement with a number of measured physical properties.

Table 1. Parameters Obtained by Fitting Resistivity Data for Ex-PAN Fibers (Spain, Volin, Goldberg and Kalnin, ref. 9). (T = 300K).

T_{HT} (^{o}C)	ρexp. ($\mu\Omega$m)	$(n+p)^*$ (10^{24}m^{-3})	v_F^* (m/s)	τ^* (10^{-14}s)	Λ^* (nm)
(1,300	15	9.4	1.0	0.3	3)†
2,200	10.5	22.	1.95	0.20	4.0
2,700	6.5	8.8	1.23	0.81	10
2,850	5.5	7.4	1.14	1.14	13
3,000	3.7	5.1	0.94	2.45	23
~3,300	3.2	4.2	0.87	3.4	30

*denotes calculated quantity

(Values derived using m* = 0.012 m$_o$)

†Values derived assuming v_F = 1.0 x 10^6 m/s

Table 1 summarizes data on room temperature resistivity, carrier density, mean-free path and relaxation time for ex-PAN fibers with 1300 < T_{HT} < 3500°C. The results were obtained using the STBM with m* = 0.012 m$_O$, which gives a reasonable value of the electronic density of states. The results show that the carrier speed is close to the value predicted from the turbostatic model (10^6 m/s). Values of parameters for the fiber with T_{HT} = 1300°C

are tentative, because the fundamental criterion for the applicability of a band model, $k_F\Lambda > 1$, where k_F is the Fermi wavenumber and Λ is the mean-free path, is not satisfied. The tabulated results for this sample are presented assuming that the mean free path is equal to L_a and that $v_F = 10^6$ m/s.

A similar analysis has been obtained on CCVD filaments by Heremans,[10] whose resistivity data are presented in Fig. 2.4. He used the STBM with the density of electrons and holes that of single-crystal graphite (2.9×10^{24} m^{-3} at T = 0°K), and a band-overlap of 18 meV (this is equivalent to assuming that $m^* = 0.013$ mg). The value of the band overlap is probably a reasonable assumption only for the filaments with $T_{HT} > 2000$°C, with resistivity values interpolated from his figure.

Table 2. Parameters Obtained by Fitting Resistivity Data for CCVD Filaments (Heremans, ref. 10)

T_{HT} (°C)	ρ ($\mu\Omega$m)	μ (m^2/vs)	τ (10^{-14}s)	Λ (nm)
3000	0.60	0.71	5.2	26
2600	0.82	0.52	3.8	19
2200	3.4	0.125	0.92	4.6
2000	8.0	0.053	0.39	1.9

E_F = Fermi Energy = 9 meV

Δ = Band Overlap = $2E_F$ = 18 meV

n (°K) = p (°K) = 2.9×10^{24}m^{-3}

V_F = 4.9×10^6 m/s

m^* = 0.013 m$_o$

(All data for 300°K)

The high temperature data of Heremans et al.[11] is analyzed using the STBM model as adapted by Heremans.[10] Only the sample with T_{HT} = 2000° is analyzed, since those with higher T_{HT} would anneal (and change their electrical characteristics in the process) at the temperature of the experiment. Also, filaments with higher T_{HT} are difficult to prepare due to the high furnace operating conditions (and are therefore extremely expensive). Resistivity values are interpolated from his curve using the formula

$$\rho = 0.55 + 2.6. \ 10^{-4}T \ (300 < T < 3000 \ K) \qquad (2.14)$$

and Eq. (2.9) for the density of carriers. The results are shown in Table 3.

Table 3. Parameters for a CCVD Filament with T_{HT} = 2800°C

T (K)	ρ ($\mu\Omega$m)	n (10^{24}m^{-3})	τ (10^{-14}s)	Λ (nm)
300	0.63	7.3	5.0	25
1000	0.81	21	1.4	6.8
2000	1.07	40	0.54	2.7
3000	1.33	59	0.29	1.4

[Resistivity values interpolated from Heremans et al., ref. 11, and values of n using Heremans, ref. 10, Eq. (1)].

Since the electrical properties of various carbons scale with the resistivity, it is reasonable to use the data in Tables 1-3 for other fiber types with the same resistivity, and to interpolate between values.

3.0 METHOD OF ANALYSIS

3.1 The Modified Drude Equations

The Drude equations for the real and imaginary parts of the
dielectric constant discussed in Section 2 are given below for
convenience:

$$\epsilon' - 1 = -(\sigma/\omega\epsilon_o)\{(\omega\tau)/[1+(\omega\tau)^2]\}, \qquad (3.1)$$

$$\epsilon'' = (\sigma/\omega\epsilon_o)\{1/[1+(\omega\tau)^2]\}, \qquad (3.2)$$

It was pointed out in Section 1 that these equations provide a
good match to the experimentally derived data of the University
of Missouri (UM) group[3] as long as the quantity $(\omega\tau)$ is not too
large. The parameters σ and τ are adjusted by them for the
correct low frequency $(\omega\tau \ll 1)$ behavior, and for the correct value
of τ for which the changes of slope (on a log-log plot) occur in
$\epsilon'(\omega)$ and $\epsilon''(\omega)$ as we move to the higher frequencies. These
changes obviously occur at the frequency for which $\omega\tau = 1$.
However, as pointed out in Section 1, the Drude model fit to the
experimentally derived data is in general poor in the frequency
range for which $\omega\tau \gg 1$. This is not surprising since the onset of
quantum mechanical effects, such as interband transitions,
commonly occurs in this range of the infrared spectrum.

As mentioned above, the UM values of conductivity σ and relaxation time τ were obtained by essentially curve fitting techniques (including but not exclusively Kramers-Kronig). In this present work, we go a step further, and write simple expressions for $\epsilon'(\omega)$ and $\epsilon''(\omega)$ that fit the data quite well throughout the range $1>>(\omega\tau)>>1$. These new Modified Drude Equations are given below:

$$\epsilon'-1=-(\sigma/\omega\epsilon_o)\{(\omega\tau)/[1+(\omega\tau)^{\alpha 1}]\}, \qquad (3.3)$$

$$\epsilon''=(\sigma/\omega\epsilon_o)\{1/[1+(\omega\tau)^{\alpha 2}]\}, \qquad (3.4)$$

where α_1 and α_2 are adjustable constants. In the Drude equations, these are both equal to 2. In the more general present case, we find these to be

$$\alpha_1=\{\ln[(\sigma/\omega\epsilon_o)(\omega\tau/[1-\epsilon'])-1]\}\{\ln(\omega\tau)\}^{-1}, \qquad (3.5)$$

$$\alpha_2=\{\ln[(\sigma/\omega\epsilon_o)(1/\epsilon'')-1]\}\{\ln(\omega\tau)\}^{-1}. \qquad (3.6)$$

It is easily seen in Eqs. (3.3) and (3.4) that, in the frequency range for which $\omega\tau>>1$, the constants α_1 and α_2 can be independently adjusted for the optimum (log-log) matching of the slopes of the experimentally derived values of $\epsilon'(\omega)$ and $\epsilon''(\omega)$ for a particular material. Note also that such adjustments do not change the frequency for which $\omega\tau=1$, nor do they change the values of $\epsilon'(\omega)$ and $\epsilon''(\omega)$ in the range $\omega\tau<<1$.

22

3.2 The Reduced Conductivity

As discussed in Section 2, when the diameter of a conducting wire is on the order of or less than the electron mean free path in the bulk material, and if the collisions with the surface are not completely elastic, then the effective value of the mean free time τ is reduced. Since the electrical conductivity σ is proportional to τ, a corresponding reduction in σ will occur. Some of the filament types that we are interested in regarding electromagnetic scattering and absorption have diameters in this size range. It is therefore essential that we include these effects in our calculations of the complex dielectric constant.

It is important to note that, in the frequency range $\omega\tau \ll 1$, the relaxation time does not explicitly appear in the Drude equation for ϵ'. In this range, we need only consider the reduction in conductivity since $|\epsilon''| \gg |\epsilon'|$ and the dielectric constant is almost pure imaginary. However, when $\omega\tau \geq 1$, we must explicitly take into account the changes in both σ and τ. It is for this reason that it was considered important to preserve the essential meaning (albeit semi-empirical) of the relaxation time.

Recognizing that the reason for the reduction in conductivity is due to an equivalent reduction in τ, we simply reduce the value of the bulk relaxation time by the same factor by which the bulk value of conductivity is reduced. This, in effect, keeps the number density of electrons independent of τ, as it should be. We thus obtain explicit new values for σ and τ for use in the Modified Drude Eqs. (3.3) and (3.4). The means by which these new values are computed is outlined in Section 2.

23

3.3 Integration of the Computations

In Figure 3.1, we show schematically how the computational elements discussed above are integrated into our present computational program for scattering/absorption by conductive filaments. Although, in view of the previous discussions, the figure is self-explanatory, we will briefly discuss it:

(1) The required input parameters for the computation of reduced conductivity and relaxation time are the fiber radius and the bulk values of conductivity, mean free time, and mean free path (which is the product of the Fermi velocity and the mean free time). The value of the assumed surface accommodation coefficient, which we label Eps must also be input. The output quantities are the reduced values of σ and τ. If the wire diameter is much greater than the mean free path Λ then σ and τ will be very nearly equal to their bulk counterparts.

(2) The material parameters needed for the computation of α_1 and α_2 are the bulk values of conductivity and relaxation time. In addition, a single experimental point at a given frequency in the $\omega\tau \gg 1$ range is required for ϵ' and another for ϵ''. The frequencies ω_1 and ω_2 need not be the same. The computed values of α_1 and α_2 guarantee that the ϵ',ϵ'' curves resulting from the use of the Modified Drude Equations will include the points $\epsilon_1(\omega_1)$ and $\epsilon_2(\omega_2)$. This is a one-time computation for each material.

(3) The Modified Drude Eqs. (3.3) and (3.4) require as inputs the size corrected values of σ and τ, as well as the computed values of α_1 and α_2. The outputs of this computational block are numerical computations of $\epsilon'(\lambda)$ and $\epsilon''(\lambda)$ over a wavelength range from many meters to very nearly the visible spectrum.
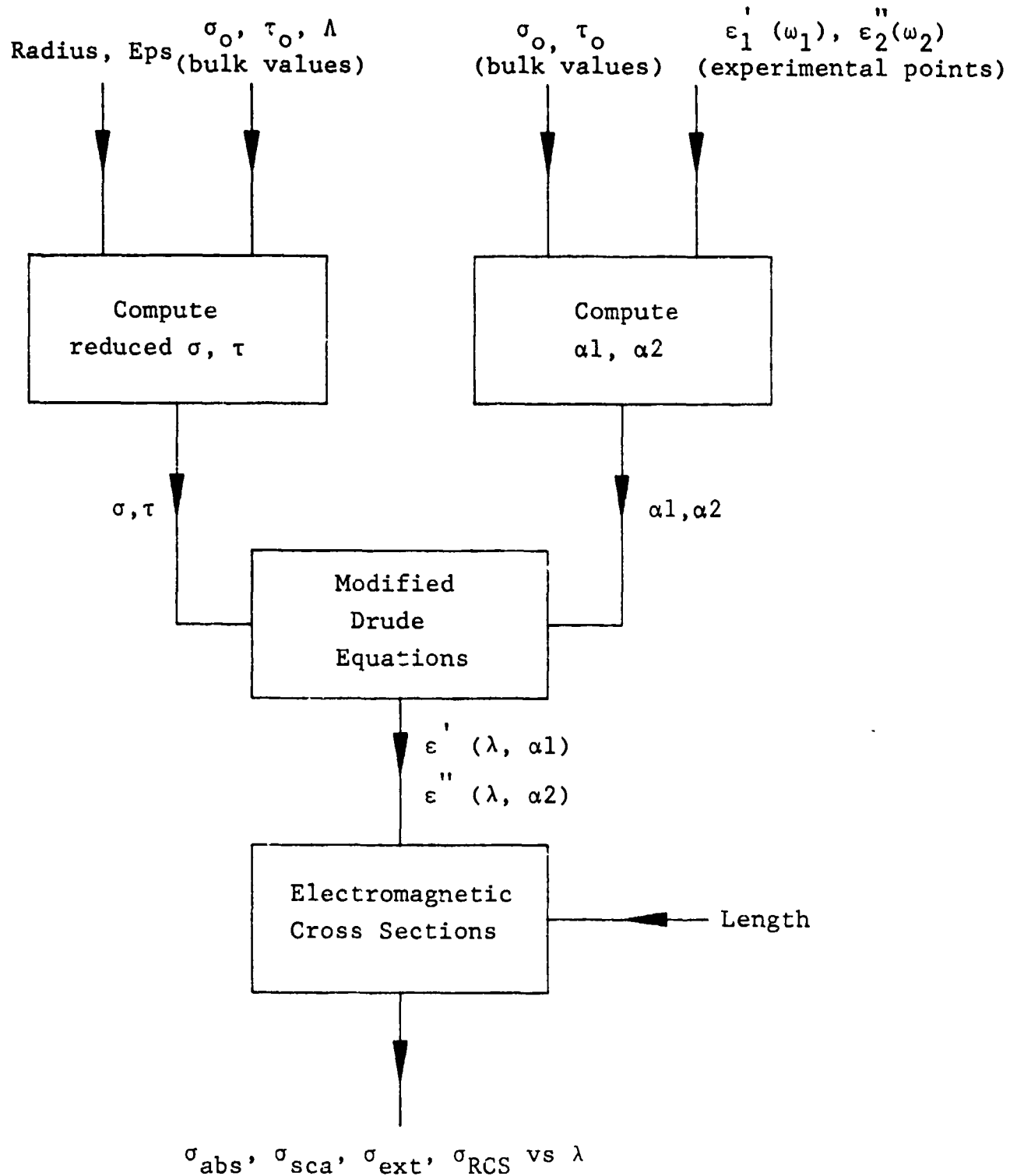
Figure 3.1 Block diagram of the overall method of computation.

(4) The $\epsilon'(\lambda)$ and $\epsilon''(\lambda)$ from (3) above, as well as particle length and radius, serve as the essential inputs for the computation of absorption, scattering, extinction, and backscatter cross sections. The particle orientation is random and the spatial distribution can be either three or two-dimensional. Polarization of the incident wave is accounted for, and we can provide data corresponding to a Gaussian distribution of particle length in the aggregate of particles.

4.0 RESULTS

The purposes of this section are twofold. First, we will provide comparative results that quantitatively demonstrate the consequences of the use of the Modified Drude Equations and the corrections of conductivity and mean free time for particles having extremely small diameters. The second purpose is to provide new quantitative predictions of the resulting electromagnetic cross sections for particle types of current interest.

Two quite different types of material are used as examples. These are pure and irradiated (or alloyed) copper, and two types of graphite fiber: (a) very small diameter CCVD, and (b) the standard commercial ex-PAN, both of which are discussed in Section 2.2.

Two types of graphical results are presented. These are for complex dielectric constant (including plots of the unmodified Drude equations for comparison), and plots of the electromagnetic cross sections, which are of course the end product of our work.

The wavelength range, although arbitrary at the long wavelength extreme, is limited to 0.5 micron at the short wavelength extreme. We feel confident about the ϵ values down to 1.0 micron, but include the range $.5\mu \leq \lambda \leq 1.0\mu$ with a word of caution.

The values of α_1 and α_2 for copper were obtained through the use of Table 1 and Table 2 of Ref.3. The reference wavelengths that were used are 1.0 μ for the computation of α_1 and 2.0 μ for the computation of α_2.

Three values of the surface accommodation coefficient (see Section 2.1) are used in the computations. These are 0, 0.5, and 1.0. The value of this quantity in practical cases is not well known.

27

4.1 Nomenclature Used in the Graphs

In the graphical results to be presented, we have included all input parameters, as well as the numerical results of some of the intermediate computations for ease of interpretation. We have thus endeavored (at the expense of a certain amount of clutter) to include all pertinent parameters in the graphs. We have found this to be very useful when comparing computational data and analyzing results. The following Table interprets the nomenclature used in the graphs to be presented in Section 4.2.

Table 4
Nomenclature (MKS units)

Conb = electrical conductivity of the bulk material.

Cond = electrical conductivity of the fiber in the small diameter regime.

Taub = electron mean free (relaxation) time in the bulk material.

~u = electron mean free time of the fiber in the small diameter regime.

m.f.p. = electron mean free path. Bulk parameter.

Kappa = ratio of particle diameter to m.f.p.

Eps = surface accommodation coefficient (0,.5,or 1).

Ratio = Cond/Conb, which is the same as Tau/Taub.

$\alpha_{1,2}$ = exponents used in the Modified Drude Equations for ϵ' and ϵ'', respectively.

28

4.2 Computational Results

4.2.1 Copper

We first present data in Fig. 4.1 for ϵ' and ϵ'' for pure copper for the case Eps=1 (no inelastic scattering at the boundary; equivalent to the properties in the large diameter regime). The departure from the Drude model predictions is seen to be negligible in the $\omega\tau \leq 1$ regime. The slope departures in the $\omega\tau > 1$ range are due to the values of α_1 and α_2 that were derived from Ref. 3, Table 2.

Using the data of Fig. 4.1 for comparison, we next assume completely _inelastic_ scattering at the boundary (Eps=0). This case is shown in Fig. 4.2. We see that, for this 50 Angstrom diameter particle, (a) the wavelength at which $\omega\tau=1$ has shifted from about 200 μ to about 5μ, and (b) the values of ϵ' and ϵ'' are larger than the Drude predictions in the $\omega\tau > 1$ range, and smaller in the $\omega\tau < 1$ range. In the case of this Figure, note that inelastic scattering at the particle boundary dominates the dielectric properties of the particle.

Next, choosing the intermediate value for the surface accommodation coefficient (Eps=0.5) and keeping all other parameters the same as above, Fig. 4.3 and 4.4 show the resulting dielectric constant behavior and the electromagnetic scattering, absorption, extinction, and backscatter (RCS) cross sections for a particle whose length is 2 microns and whose diameter is 50 Angstroms and whose (total) length is 2 microns.

Note that, in Fig. 4.4, the extinction is almost entirely due to absorption. If the diameter of this particle were made sufficiently greater, the extinction would be primarily due to scattering. If its length were increased, the extinction peak at about 50 μ would move to a longer wavelength.

PLOTS OF DIELECTRIC CONSTANT INCLUDING DIMENSIONAL EFFECTS
Cylindrical particle. Material: Copper; Radius= 2.5E-09 m

ABS(Re(Epsilon))
Im(Epsilon)
Drude eqn's

PANAMETRICS
Program:
EPSILON
21 Aug 1988

PARAMETERS:
(MKS UNITS)
Conb=8.1E+07
Cond=8.1E+07
Taub=7.2E-14
Tau=7.2E-14
m.f.p.=1.1E-07
Kappa=4.4E-02
Eps=1.0E+00
Ratio=1.0E+00
Alpha1=1.88
Alpha2=1.43
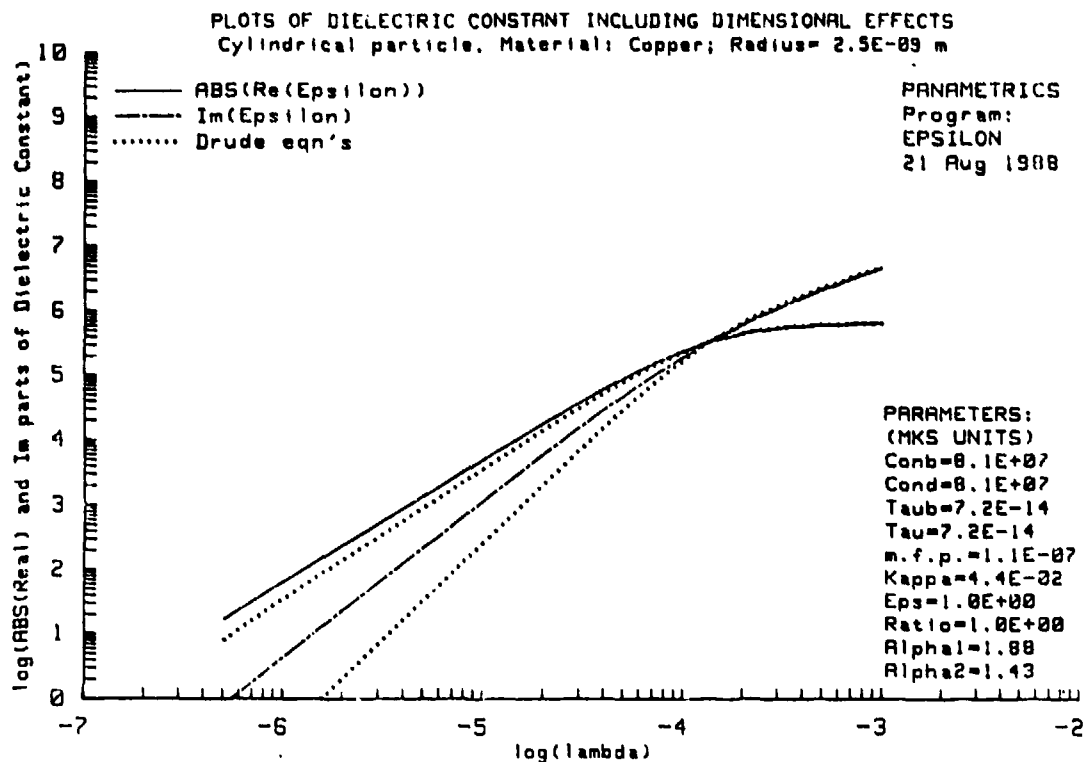
Fig. 4.1. ϵ' and ϵ'' vs λ for a thin copper filament. No inelastic boundary scattering (Eps=1).

PLOTS OF DIELECTRIC CONSTANT INCLUDING DIMENSIONAL EFFECTS
Cylindrical particle. Material: Copper; Radius= 2.5E-09 m

ABS(Re(Epsilon))
Im(Epsilon)
Drude eqn's

PANAMETRICS
Program:
EPSILON
21 Aug 1988

PARAMETERS:
(MKS UNITS)
Conb=8.1E+07
Cond=3.3E+06
Taub=7.2E-14
Tau=3.0E-15
m.f.p.=1.1E-07
Kappa=4.4E-02
Eps=0.0E+00
Ratio=4.1E-02
Alpha1=1.88
Alpha2=1.43
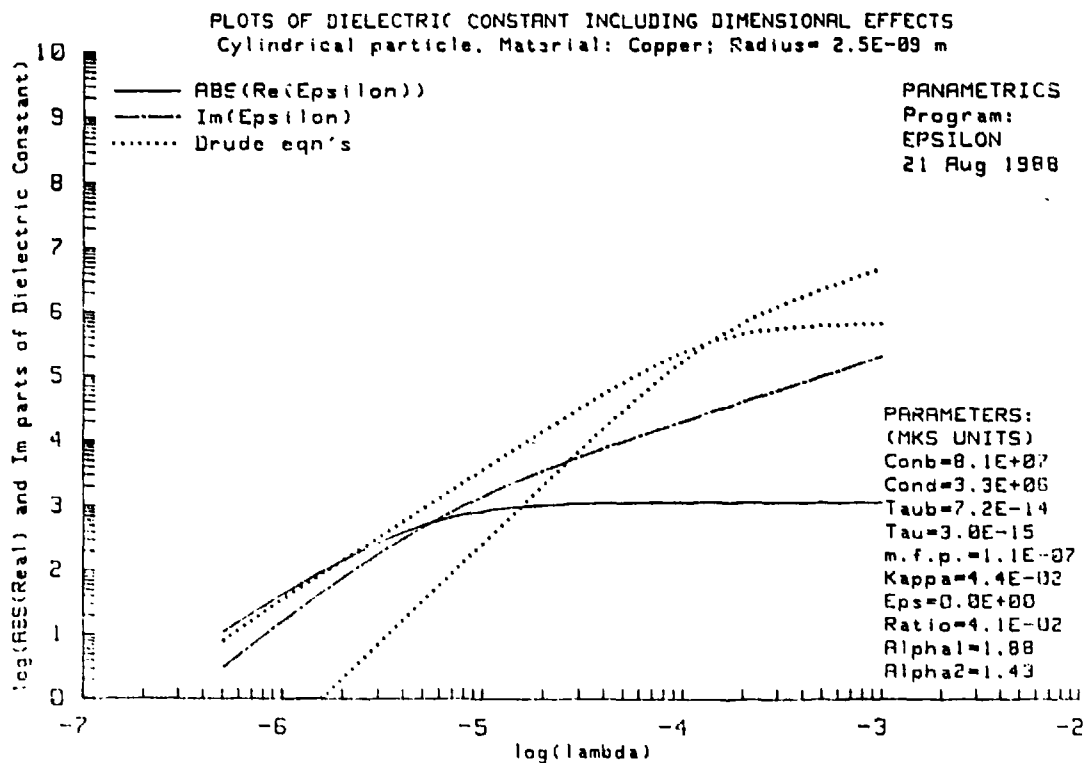
Fig. 4.2. ϵ' and ϵ'' vs λ for the thin copper filament. Totally inelastic boundary scattering (Eps=0).

PLOTS OF DIELECTRIC CONSTANT INCLUDING DIMENSIONAL EFFECTS
Cylindrical particle. Material: Copper; Radius= 2.5E-09 m

ABS(Re(Epsilon))
Im(Epsilon)
Drude eqn's

PANAMETRICS
Program:
EPSILON
21 Aug 1988

PARAMETERS:
(MKS UNITS)
Conb=8.1E+07
Cond=8.6E+06
Taub=7.2E-14
Tau=7.7E-15
m.f.p.=1.1E-07
Kappa=4.4E-02
Eps=5.0E-01
Ratio=1.1E-01
Alpha1=1.88
Alpha2=1.43

log(ABS(Real) and Im parts of Dielectric Constant)

log(lambda)

Fig. 4.3. ϵ' and ϵ'' vs λ for the thin copper filament (Eps=0.5).

PLOTS OF LENGTH-AVERAGED ELECTROMAGNETIC CROSS SECTIONS VS WAVELENGTH
3-D Data, MKS Units. Standard deviation of length= 2.00E-07 m

Material: Copper

PANAMETRICS
Program:
JNP_BW2
20 Aug 1988

Extinction
Absorption
Scattering
R.C.S.

PARAMETERS
radius=2.5E-09
length=2.0E-06
cond.=8.6E+06
tau=7.7E-15
mfp=1.1E-07
Eps=5.0E-01
Kappa=4.4E-02
Ratio=1.1E-01

log(Cross Sect/unit vol)

X=1

log(lambda)

Fig. 4.4. Electromagnetic cross sections for the thin copper
filament (Eps=.5).

31

Figures 4.5 and 4.6 pertain to a pure copper particle having a radius of 0.1 μ and length of 2 μ, and Eps=0.5. Note that, due to the relatively large radius, the conductivity and mean free path are 90% (Ratio=.90) of their bulk values. As discussed above, note that the scattering now (as compared with Fig. 4.4) dominates the extinction. Note also that the extinction peak is narrower and is smaller in magnitude by more than an order of magnitude.

We next consider a hypothetical case in which the copper fiber of Fig.'s 4.5 and 4.6 is irradiated in a nuclear reactor or, alternatively, alloyed with a small amount of impurity. We assume that such treatment could result in a decrease in τ by a factor of 100, but that the number density and effective mass of the carriers would be unaltered by this conditioning. The resulting dielectric constant and electromagnetic cross sections are shown in Figures 4.7 and 4.8. Note that, since we have no experimental data available for this hypothetical material, we have little choice but to let $\alpha_1 = \alpha_2 = 2$. Note also that the conditioning of the copper has resulted in $\omega\tau = 1$ at approximately $\lambda = 1.5\mu$.

PLOTS OF DIELECTRIC CONSTANT INCLUDING DIMENSIONAL EFFECTS
Cylindrical particle. Material: Copper; Radius= 1.0E-07 m

ABS(Re(Epsilon))
Im(Epsilon)
Drude eqn's

PANAMETRICS
Program:
EPSILON
21 Aug 1988

PARAMETERS:
(MKS UNITS)
Conb=8.1E+07
Cond=7.3E+07
Taub=7.2E-14
Tau=6.5E-14
m.f.p.=1.1E-07
Kappa=1.8E+00
Eps=5.0E-01
Ratio=9.0E-01
Alpha1=1.88
Alpha2=1.43

log(lambda)

Fig. 4.5. ε' and ε'' vs λ for a thick copper filament.

PLOTS OF LENGTH-AVERAGED ELECTROMAGNETIC CROSS SECTIONS VS WAVELENGTH
3-D Data, MKS Units. Standard deviation of length= 2.00E-07 m

Material: Copper

PANAMETRICS
Program:
JNP_BW2
20 Aug 1988

Extinction
Absorption
Scattering
R.C.S.

PARAMETERS
radius=1.0E-07
length=2.0E-06
cond.=7.3E+07
tau=6.5E-14
mfp=1.1E-07
Eps=5.0E-01
Kappa=1.8E+00
Ratio=9.0E-01

log(lambda)

Fig. 4.6. Electromagnetic cross sections for the thick copper
filament of Fig 4.5.

33

PLOTS OF DIELECTRIC CONSTANT INCLUDING DIMENSIONAL EFFECTS
Cylindrical particle. Material: Irradiated Copper; Radius= 1.0E-07 m

ABS(Re(Epsilon))
Im(Epsilon)
Drude eqn's

PANAMETRICS
Program:
EPSILON
21 Aug 1988

PARAMETERS:
(MKS UNITS)
Conb=8.1E+05
Cond=8.1E+05
Taub=7.2E-16
Tau=7.2E-16
m.f.p.=1.1E-09
Kappa=1.8E+02
Eps=5.0E-01
Ratio=1.0E+00
Alpha1=2.00
Alpha2=2.00

log(ABS(Real)) and Im parts of Dielectric Constant

log(lambda)

Fig. 4.7. ϵ' and ϵ'' vs λ for a hypothetical irradiated thick copper filament.

PLOTS OF LENGTH-AVERAGED ELECTROMAGNETIC CROSS SECTIONS VS WAVELENGTH
3-D Data. MKS Units. Standard deviation of length= 2.00E-07 m

Material: Irradiated Copper

PANAMETRICS
Program:
JNP_BW2
20 Aug 1988

Extinction
Absorption
Scattering
R.C.S.

PARAMETERS
radius=1.0E-07
length=2.0E-06
cond.=8.1E+05
tau=7.2E-16
mfp=1.1E-09
Eps=5.0E-01
Kappa=1.8E+02
Ratio=1.0E+00

log(Cross Sect/unit vol)

log(lambda)

Fig. 4.8 Electromagnetic cross sections for the hypothetical irradiated thick copper filament.

34

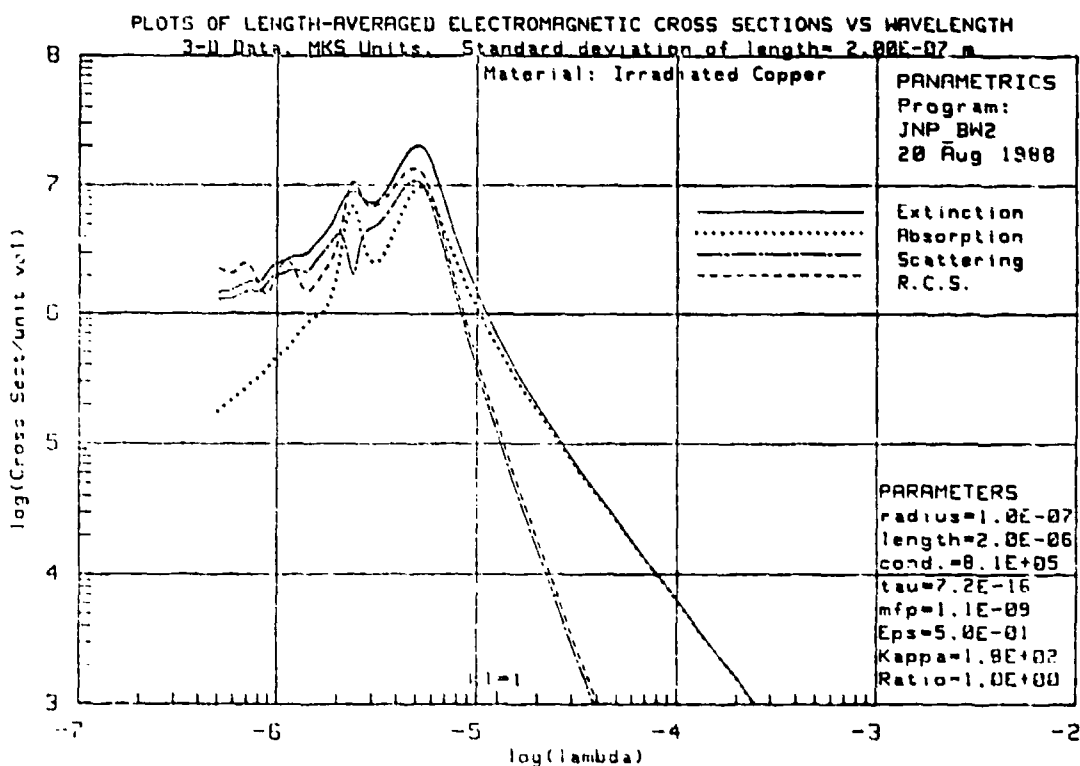## 4.2.2 Graphite Fibers

The best data available at this time on the electrical properties of graphite fibers is contained in the tables of Section 2.2, which was authored by Prof. Ian Spain, Dept. of Physics, Colorado State University. Professor Spain, a leading expert in graphite fiber technology, has been a Panametrics consultant for about three years.

Although we can directly utilize the data of Section 2.2 in our calculations of ϵ' and ϵ'', it is an unfortunate fact that no experimental data presently exists for these quantities in the near infrared. This means that, although the tabulated σ and τ values are probably good numbers, we do not know the (log-log) slopes of ϵ' and ϵ'' vs λ in the $\omega\tau \gg 1$ region as we do in metals, e.g. the case of copper. Therefore, we have, as in the hypothetical case of irradiated copper, little choice but to let $\alpha_1 = \alpha_2 = 2$ for the graphite fibers considered herein.

With this in mind, we first take the case of ex-PAN fibers that have been subjected to two annealing temperatures: 2200 and 3300°C. These are designated PAN2200 and PAN3300 respectively. The dielectric constant and resulting electromagnetic cross sections (3 μ diameter and 10 μ total length) for PAN2200 fibers are given in Fig.'s 4.9 and 4.10. The results for the case of PAN3300 are given in Fig.'s 4.11 and 4.12.

Comparing the ϵ', ϵ'' curves of Fig 4.9 and 4.11, we see that the difference in annealing temperatures results in quite significant differences in the respective ϵ plots. We were therefore somewhat surprised to find that only subtle differences are seen in the respective electromagnetic cross sections of Fig.'s 4.10 and 4.12. If, however, the particle length were sufficiently increased, the low frequency behaviors would exhibit much greater differences.
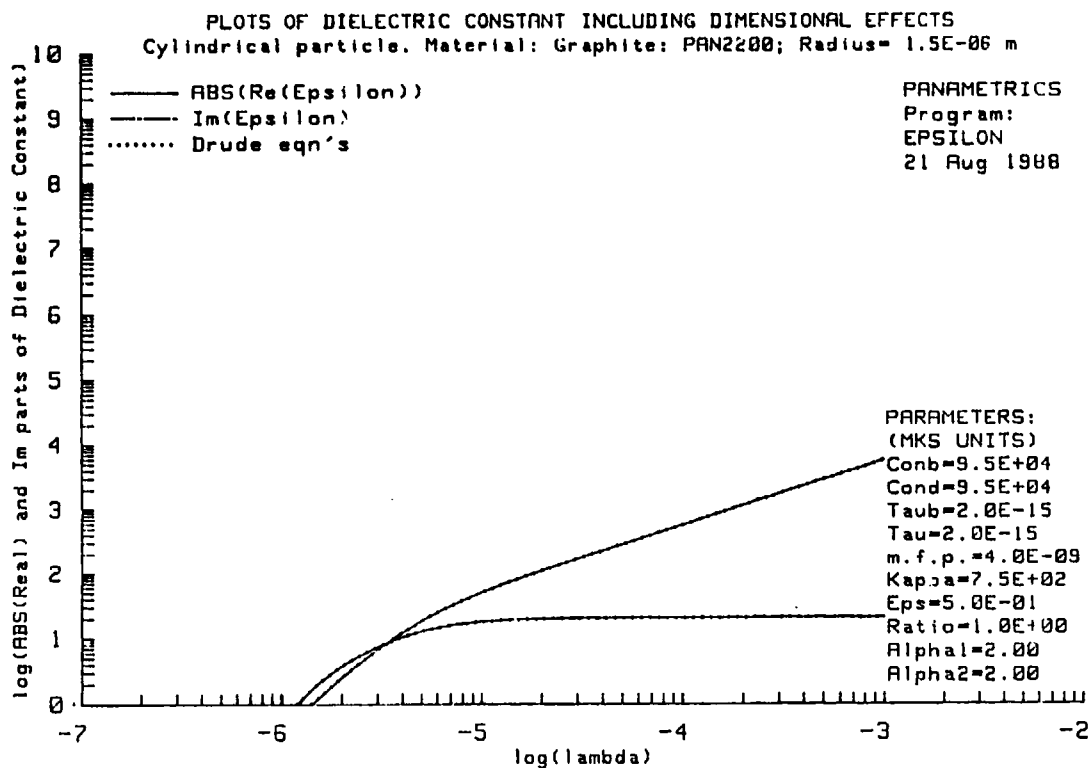
PLOTS OF DIELECTRIC CONSTANT INCLUDING DIMENSIONAL EFFECTS
Cylindrical particle. Material: Graphite: PAN2200; Radius= 1.5E-06 m

——— ABS(Re(Epsilon))
—·—· Im(Epsilon)
········ Drude eqn's

PANAMETRICS
Program:
EPSILON
21 Aug 1988

PARAMETERS:
(MKS UNITS)
Conb=9.5E+04
Cond=9.5E+04
Taub=2.0E-15
Tau=2.0E-15
m.f.p.=4.0E-09
Kappa=7.5E+02
Eps=5.0E-01
Ratio=1.0E+00
Alpha1=2.00
Alpha2=2.00

Fig.4.9. ε' and ε'' vs λ for PAN2200 graphite fibers.

PLOTS OF LENGTH-AVERAGED ELECTROMAGNETIC CROSS SECTIONS VS WAVELENGTH
3-D Data. MKS Units. Standard deviation of length= 1.00E-05 m

Material: Graphite: PAN2200

PANAMETRICS
Program:
JNP_BW2
20 Aug 1988

———— Extinction
········ Absorption
—·—· Scattering
——— — R.C.S.

PARAMETERS
radius=1.5E-06
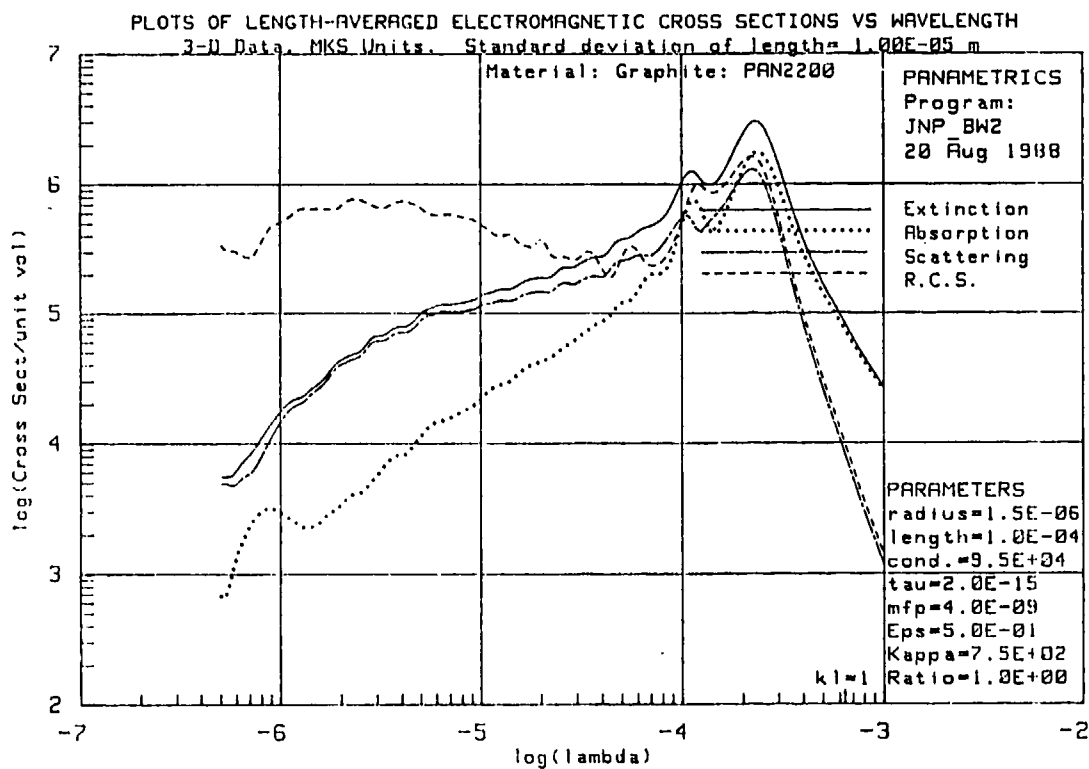length=1.0E-04
cond.=9.5E+04
tau=2.0E-15
mfp=4.0E-09
Eps=5.0E-01
Kappa=7.5E+02
kl=1 Ratio=1.0E+00

Fig.4.10. Electromagnetic cross sections for PAN2200 graphite
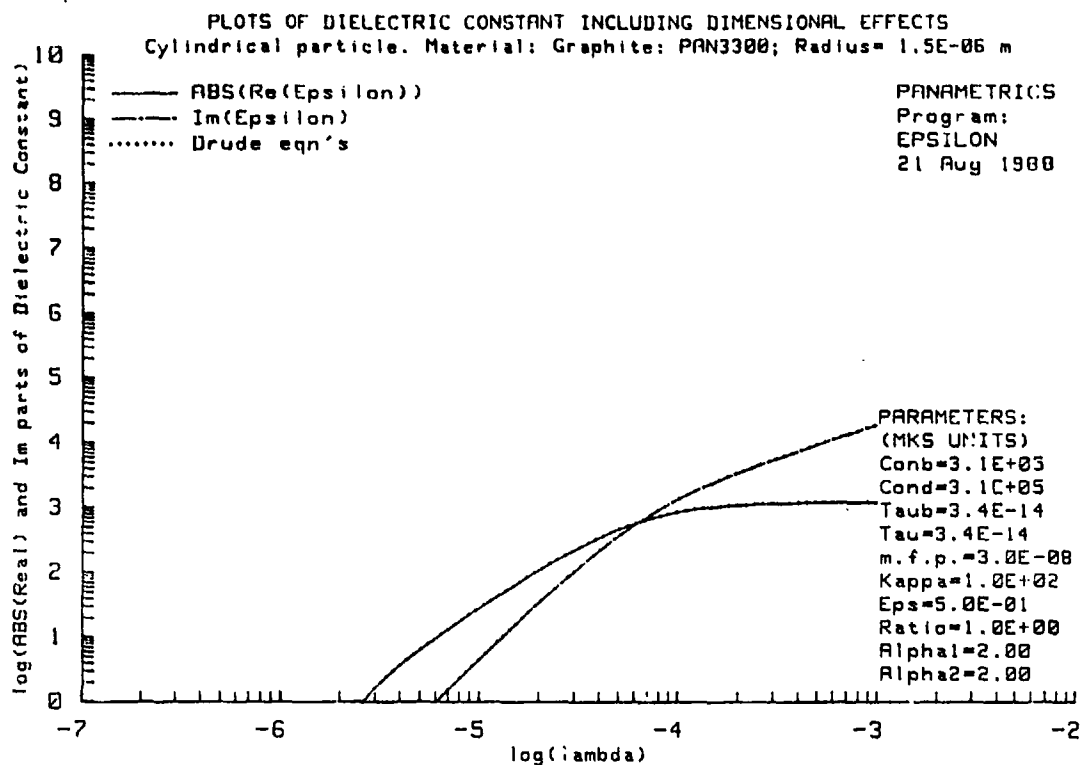fibers. Length=100 microns, diameter=3 microns.

36

PLOTS OF DIELECTRIC CONSTANT INCLUDING DIMENSIONAL EFFECTS
Cylindrical particle. Material: Graphite: PAN3300; Radius= 1.5E-06 m

Fig.4.11. ϵ' and ϵ'' vs λ for PAN3300 graphite fibers.

PLOTS OF LENGTH-AVERAGED ELECTROMAGNETIC CROSS SECTIONS VS WAVELENGTH
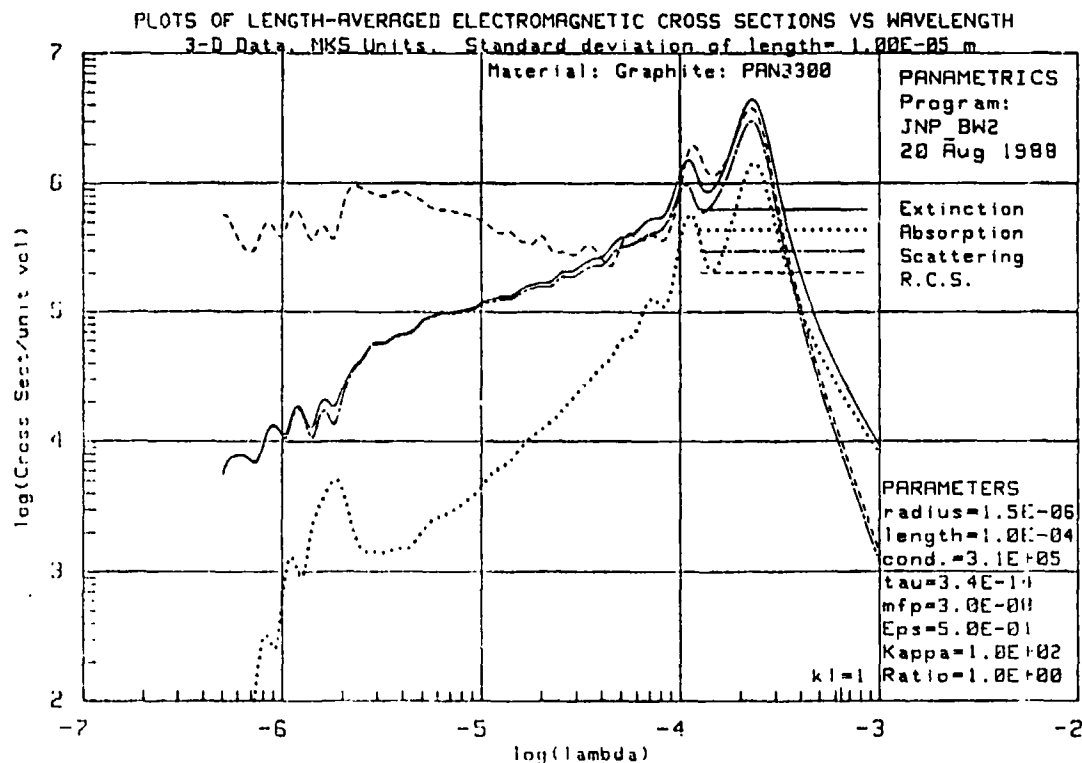3-D Data. MKS Units. Standard deviation of length= 1.00E-05 m

Fig 4.12. Electromagnetic cross sections for PAN3300
graphite filaments.

Our final set of plots, Fig.'s 4.13 and 4.14, is for CCVD graphite fibers, which have very much smaller dimensions than the ex-PAN variety. For this fiber, we assume an annealing temperature of 2000°C, and a length and diameter of 2 microns and 100 Angstroms, respectively. We see that this fiber produces a much broader (absorption dominated) extinction cross section and that the magnitude of the extinction cross section/unit volume is an order of magnitude higher than the ex-PAN fibers. This latter feature is without question partly due to the fact that the PAN fibers are either too short or too thick, and partly due to the higher bulk conductivity of the CCVD fiber.
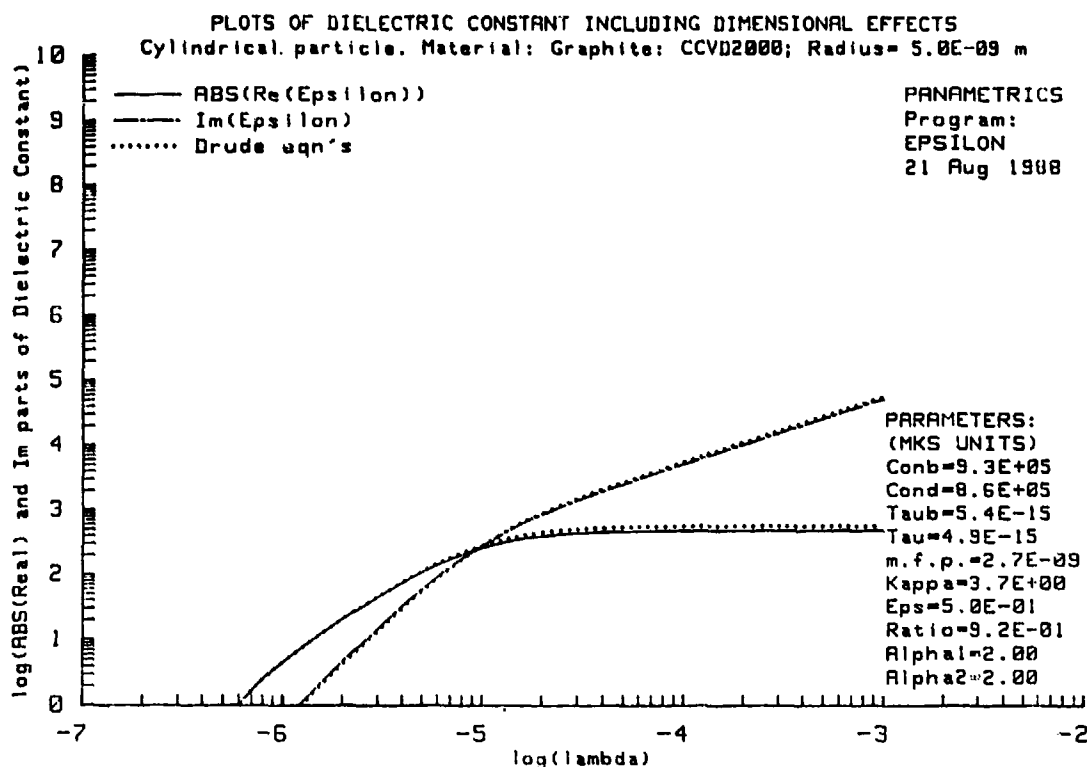
PLOTS OF DIELECTRIC CONSTANT INCLUDING DIMENSIONAL EFFECTS
Cylindrical particle. Material: Graphite: CCVD2000; Radius= 5.0E-09 m

Fig. 4.13. ϵ' and ϵ'' vs λ for CCVD2000 graphite fibers.
Radius=50 Angstroms.

PLOTS OF LENGTH-AVERAGED ELECTROMAGNETIC CROSS SECTIONS VS WAVELENGTH
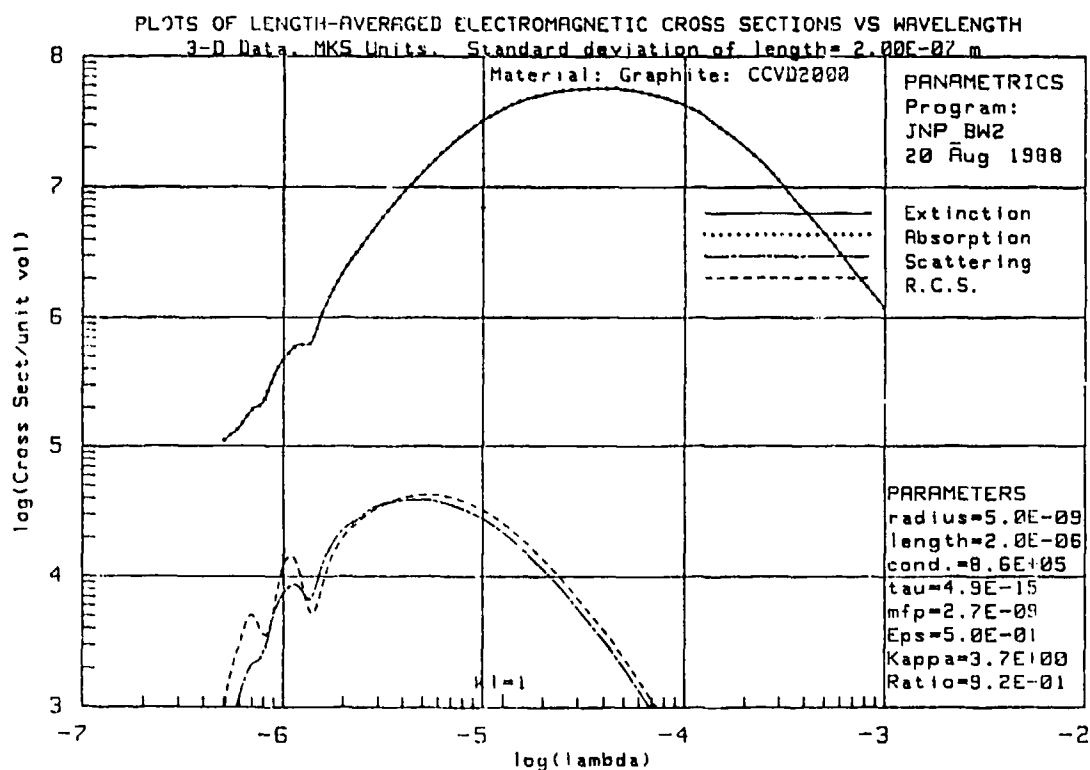3-D Data, MKS Units. Standard deviation of length= 2.00E-07 m

Fig. 4.14. Electromagnetic cross sections for the CCVD2000
filament. Length=2 microns.

5.0 DISCUSSION AND CONCLUSIONS

At the beginning of this Program, we did not have very much confidence in our abilit" to quantitatively predict electromagnetic cross sections of conductive filaments for wavelengths less than 5u or so microns. At longer wavelengths, our confidence has been high. With the conclusion of the present work, we now have a much higher level of confidence in our predictions over the wavelength range essentially "from DC to light" in the case of those metals for which sufficient optical data exists. This has been made possible by providing two new independent adjustable parameters in the Drude equations. The resulting Modified Drude Equations utilize the previous[3] (essentially empirically) optimized values of DC conductivity and relaxation time, but also include two new parameters, α_1 and α_2 that provide good fits to the experimental data in the short wavelength ($\omega\tau \gg 1$) regime. The metals for which this procedure is appropriate are: Al, Co, Cu, Au, Fe, Pb, Ni, Pd, Pt, Ag, Ti, and W.

We have also included the computational capability to take into account the reduction of electrical conductivity and relaxation time due to inelastic collisions of conduction electrons with the filament boundary. These effects are only important when the diameter of the filament is on the order of or less than the mean free path in the bulk material. The resulting corrections are theoretically fully justified and believed to be accurate in the wavelength range for which $\omega\tau \leq 1$ in bulk material.

In the special case where (a) $\omega\tau > 1$ <u>and</u> (b) the diameter is comparable to or less than the bulk mean free path, we do not have very much confidence that the values of α_1 and α_2 are accurate. However, until we can obtain experimental infrared data in this regime, the use of our bulk values of α_1 and α_2

cannot be theoretically justified but it will have to suffice until experimental data for this regime become available. Perhaps a good approach in this regard would be to use optical data on thin metallic (planar) films, and to work out corrections due to the difference in geometry.

Metals for which the above curve fitting techniques are inappropriate are Au, Ni, and Pb. However, recent detailed tabulated data do exist for these[13] over very wide wavelength ranges extending into the visible spectrum. In these cases, we can obviously use interpolation techniques to provide correct values of ϵ' and ϵ''. However, it is difficult to see how to apply the small size corrections of the preceding paragraph in these cases, for which it is not possible to identify a relaxation time τ.

As mentioned above, we believe that optical measurements on thin films for which the thickness is on the order of or less than Λ would permit significant extension of our computational capability.

Areas of application of the present work are:

(1) Calculation of electromagnetic cross sections for conducting or non-conducting fibers having thin conductive coatings. In this case, we would use the Fuchs[5] thin film results.

(2) Improved calculations of the cross sections of flake-like, and sphere-like aerosol particles are possible. The geometries of Fuchs (one dimensional planar) or of Dingle[6] (two dimensional cylindrical) would not be appropriate for the three dimensional sphere case, and we would need to modify the geometry of either of these works for spheres. An approximate theory for this, we believe, would probably not be very difficult to derive. We believe that such a treatment would yield improved results that

41

would differ considerably from those presently available in the area of aerosol scattering and absorption.

(3) In the area of electromagnetic extinction, the notion of alloying or irradiating a very thin metallic fiber type allows for the possibility of providing optimal values of σ and τ for metallic fibers than cannot be made arbitrarily thin.

(4) The results of the present work can be directly applied to our previous[1] work in the area of thermal radiation from small absorbing particles. This application would result in greatly improved quantitative predictions of the radiation spectra of such particles.

5.1 Acknowledgements

REFERENCES

1. N. E. Pedersen, P. C. Waterman and J. C. Pedersen, "Absorption, Scattering, and Thermal Radiation by Conductive Fibers," AFOSR Final Report, Panametrics, Inc. (July 16, 1987).

2. N. W. Ashcroft and N. D. Mermin, Solid State Physics, (Holt, Rinehart and Winston, Philadelphia, 1976).

3. M. A. Ordal, R. J. Bell, R. W. Alexander, L. L. Long, and M. R. Querry, Appl. Opt. 24, 4493 (1985).

4. C. Kittel, Introduction to Solid State Physics, (J. Wiley and Sons, N.Y., 1953), p. 236.

5. K. Fuchs, Proc. Camb. Phil. Soc. 34, 100 (1938).

6. R. B. Dingle, Proc. Roy. Soc A 201, 545 (1950).

7. M. S. Dresselhaus, H. A. Goldberg and I. L. Spain, in Proc. of the 1985 CRDC Conf. on Obscuration and Aerosol Research, p. 291-324, (ed. R.H. Kohl), (1985).

8. M. S. Dresselhaus, G. Dresselhaus, K. Sugihara, I. L. Spain and H. A. Goldberg, Graphite Fibers and Filaments (Springer Verlag, Berlin, 1988).

9. I. L. Spain, Chemistry and Physics of Carbon, Vol. 16, p. 119, (1981). I. L. Spain, K. A. Volin, H. A. Goldberg and I.L. Kalnin, J. Phys. Chem. Solids, 44, 839, (1983).

10. J. Heremans, Carbon 23, 431-436, (1985).

11. J. Heremans, C. H. Olk, G. L. Eesley, J. Steinbeck and G. Dresselhaus, Phys. Rev. Lett., 60, 452, (1988).

12. A. A. Bright, Phys. Rev., B20, 5142, (1979).

13. M. A. Ordal, R. J. Bell, R. W. Alexander, Jr., L. L. Long and M. R. Querry, Appl. Opt. 26, 744 (1987).